Letter

Dual-Polarized Backscatter Features of Surface Currents in the Open Ocean during Typhoon Lan (2017)

Guosheng Zhang [1,2,*] **and William Perrie** [2]

1   Key Laboratory of Geographic Information Science (Ministry of Education), East China Normal University, Shanghai 200241, China
2   Fisheries and Oceans Canada, Bedford Institute of Oceanography, Dartmouth, NS B2Y 4A2, Canada; William.Perrie@dfo-mpo.gc.ca
*   Correspondence: zgsheng001@gmail.com; Tel.: +1-902-426-7797

check for updates

Abstract: Ocean surface current measurements from satellites have historically been limited. We propose a new approach to detect ocean surface currents as observed by dual-polarized (VV and VH) spaceborne synthetic aperture radar (SAR). This approach is based on the assumptions that the VH-polarized SAR signal is only generated by the effects of ocean winds creating surface waves, whereas the VV-polarization data are due to the effects of both ocean winds and surface currents. Therefore, the surface currents features may be extracted after retrieving the ocean winds from VH-polarized backscatter and inputting signal due to the wind to the VV-polarized backscatter data. To investigate the performance of this approach under extreme wind conditions, we consider a scene of C-band RADARSAT-2 dual-polarized ScanSAR images over Typhoon Lan (2017) in the open ocean, and we verify our results with current estimates from altimeter data. The ocean current features extracted from the backscatter data that were collected from the SAR images are shown to correspond to an area of strong currents and an oceanic front observed by altimeters. We suggest that the proposed method has the potential capacity to provide information about ocean surface currents from high-resolution dual-polarized ScanSAR images.

Keywords: ocean surface currents; typhoon impacts on the ocean; synthetic aperture radar (SAR)

1. Introduction

Observations of surface currents in the open ocean have historically been limited; high-frequency (HF) radar has been used for a limited range in coastal areas and ADCP (acoustic Doppler current profiler) and buoy deployments have provided data at specific point locations [1]. Compared to the passive remote sensing instruments that operate from satellites in the visible and infrared bands, the microwave data such as Special Sensor Microwave Imager (SSM/I), Tropical Rainfall Measuring Mission (TRMM) imagery, Quick Scatterometer (QuikSCAT), and Advanced Scatterometer (ASCAT) have the advantage of essentially being able to work in all-weather conditions, day or night, penetrating fog and cloud [2]. These instruments are sensitive to sea surface waves generated by the wind. However, it is difficult for them to detect ocean current features. For the ocean currents, spaceborne altimeters onboard satellites such as TOPEX/POSEIDON, Jason-1, Jason-2, and ERS1-2 are widely used to detect large-scale oceanic Rossby waves [3] and mesoscale eddies [4]. Until the SWOT (Surface Water and Ocean Topography) satellite is launched in 2021 (https://swot.jpl.nasa.gov), only measurements of sea surface height along points of the narrow altimeter tracks are available.

Recently, spaceborne active microwave synthetic aperture radars (SARs) have been reported as a potential tool for the detection of sea surface currents [5]. SAR techniques can be grouped into two

methodologies: (1) Doppler velocity detection, which is caused by the motions of the SAR sensor relative to the ocean surface, and (2) the SAR backscatter signal which is based on the surface wave modulations by the ocean surface currents on the Bragg resonance scales [6]. However, a stationary location (i.e., land or island) is needed for the calibration of the current measurements using Doppler velocity methods, because the motions of the sea surface on the scale of meters per second are negligible compared to the movement of the satellite SAR sensor (e.g., about 7500 m/s for RADARSAT-2).

Previous studies have used modulations by ocean currents in spaceborne SAR images to analyze the processes of ocean dynamics, i.e., the detection of oceanic fronts [7] and studies of nonlinear Ekman divergence [8]. Thus, a transfer mechanism was proposed for the modulations by ocean currents [6]. In a recent study [9], we inferred that the resonance process between ocean surface waves and the radar microwave signal mostly occurs for the backscatter signal in the VV-polarization channel, but is negligible in the VH-polarization channel. Therefore, theoretically, two-dimensional ocean surface current features and ocean winds can be extracted together from two channels (VV and VH), which are acquired simultaneously by RADARSAT-2. Moreover, the VH-polarized SAR image in RADARSAT-2 dual-polarized (VV and VH) ScanSAR mode appears not to saturate in high wind speeds under tropical cyclone (TC) conditions, and also appears to be linearly related to the ocean wind [10,11]. Because the sea surface Bragg waves on the scale of the radar microwave may interact with the surface currents [7], the radar signal of VV-polarization may be modulated by the surface currents through the Bragg resonance process. Therefore, the C-band VH-polarized radar signal is dominated by ocean wind, whereas the VV-polarized signal includes both effects of ocean winds and surface currents. For simplicity, we assume that the VH-polarized radar signal is only induced by wind, especially under the extreme TC conditions. The main goal for our study is to extract two-dimensional current features from the dual-polarized (VV and VH) SAR images at high spatial resolution. In future studies, it may be possible to combine these 'current features' with Doppler-shift information from the SAR raw data to extract the actual current speeds. This study is also motivated by the urgent need for verification observations for ocean models, especially for high spatial resolution [12].

In this study, we report a new approach for the decomposition of RADARSAT-2 dual-polarized (VV and VH) ScanSAR images over Typhoon Lan (2017) and we verify the extracted currents features with altimeter data. There are three steps for the decomposition approach: (1) retrieve wind vectors from the VH-polarized SAR image, (2) simulate the theoretical VV-polarized SAR image, and (3) extract the ocean surface current features by comparing the simulated and observed VV-polarized SAR images. Data sets of dual-polarized RADARSAT-2 ScanSAR images of Typhoon Lan (2017) and the composite five-day ocean currents from satellite altimeters are described in Section 2. The methodology we propose for the extraction of ocean surface currents from dual-polarized ScanSAR images is given in Section 3. The ocean surface currents features derived from the SAR images and the comparisons to altimeter currents are presented in Section 4. Finally, discussions and conclusions are given in Section 5.

2. Materials and Methods

2.1. Data Sets

Typhoon Lan was the third-most intense tropical cyclone worldwide in 2017. A scene of C-band dual-polarized (VV and VH) RADARSAT-2 ScanSAR images was acquired at 09:20 UTC on 21 October, 2017 over Typhoon Lan. The location of the SAR frame is shown in Figure 1. The ocean current speeds from the Ocean Surface Current Analysis (OSCAR) of 22 October, 2017 are also shown in Figure 1, which are supplied by the Physical Oceanography Distributed Active Archive Center (PO.DAAC) [13]. The OSCAR currents are estimated by using sea surface height from the satellite altimeters: TOPEX/POSEIDON, Jason-1, Jason-2, ERS1-2, GFO, and ENVISAT, as well as other measurements. The spatial grid is $1/3° \times 1/3°$ with a 5-day resolution. The currents in Figure 1 on October 22 are the composite data acquired for a period extending over five days. The Best Track of Typhoon Lan (2017) in Figure 1

is provided by the Japan Meteorological Agency (http://www.jma.go.jp/jma/jma-eng/jma-center/rsmc-hp-pub-eg/Besttracks/).
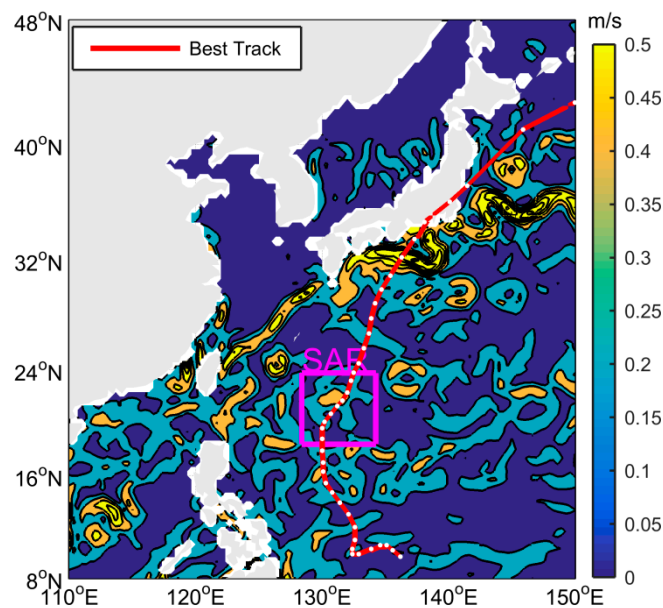
Figure 1. The dual-polarized SAR (synthetic aperture radar) image position and the best track for Typhoon Lan (2017). The background displays the OSCAR current speeds.
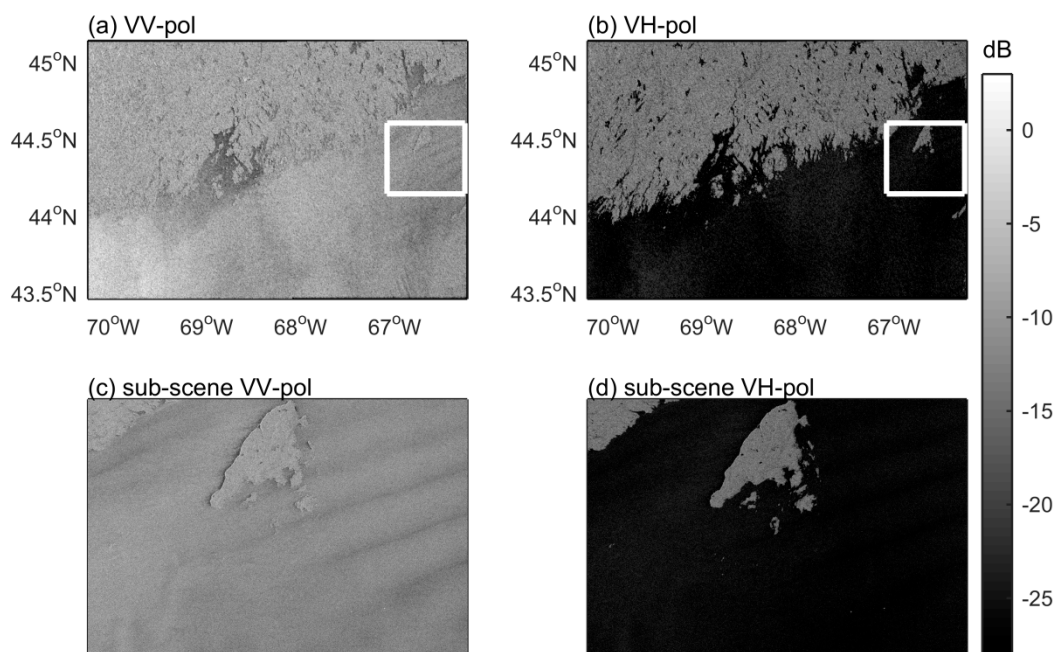
The dual-polarized (VH and VV) RADARSAT-2 ScanSAR wide imaging mode provides large swaths, high resolution, all-weather, and day-and-night surveillance, which is suitable for the accurate analysis of the ocean surface conditions under tropical cyclones (TCs). The swath width is 450 km and the pixel spacing is 50 m. The noise floor for the dual-polarization ScanSAR wide-swath data is about -29 dB, with a radiometric error that is less than 1 dB [14]. The ocean backscatter is described by the normalized radar cross section (NRCS).

Our theory model for the backscatter from ocean winds and currents is based on Bragg resonance between the sea surface waves and the radar microwaves. The sea surface waves that are induced by wind are simulated by a model for the wave spectrum. Because the wave spectrum is a statistical concept, large samples need to be acquired to provide a stable relationship between winds and sea surface waves. Thus, a particular spatial scale of the ocean surface is needed to include a sufficient amount of waves. For example, under constant, stable winds, ocean surface waves with various length scales will be generated, and various radar backscatters will be imaged by the SAR. There are no stable relationships between the wind and a *single* individual sea surface wave. We can only get a stable relationship between the wind and a spectrum of sea surface waves with various spatial scales generated by constant, stable wind conditions. Therefore, we calibrated the SAR image and then averaged the spatial resolution to 5 km using the boxcar averaging method (as shown in Figure 2). Moreover, with averaging, the SAR speckle noise is almost removed. The latitude and longitude information is also acquired with the calibration process using the transfer function provided by the Canadian Space Agency (CSA, Saint-Hubert, QC, Canada).
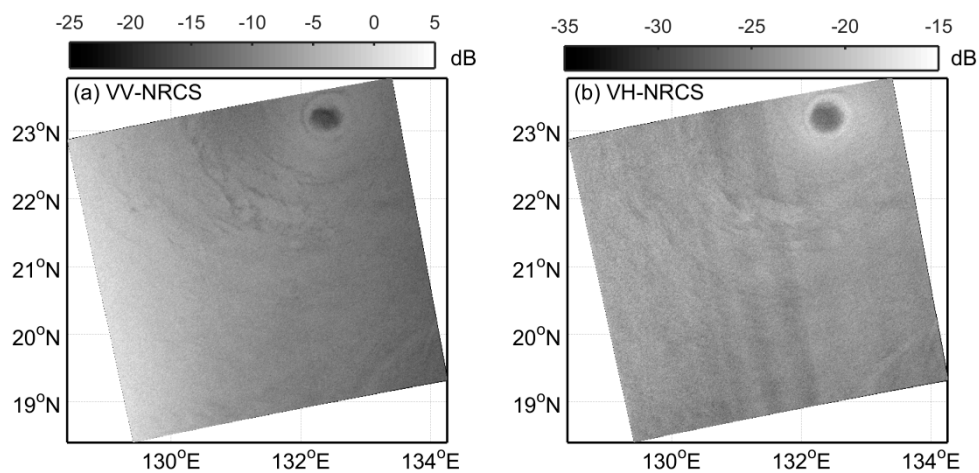
Figure 2. Dual-polarized RADARSAT-2 ScanSAR images over Typhoon Lan (09:20 UTC, 21 October 2017): (**a**) VV-polarization and (**b**) VH-polarization. RADARSAT-2 Data and Products MacDonald, Dettwiler, and Associates Ltd. (Toronto, ON, Canada), All Rights Reserved.

To further demonstrate that the current modulations are different in the different polarizations of VV and VH, we employ additional dual-polarized (VH and VV) RADARSAT-2 ScanSAR images of the Bay of Fundy (Figure 3). Because of the very high tidal range in the Bay of Fundy, the currents are very strong [15]. It is obvious that the current signatures are much clearer in the VV-pol image (Figure 3a,c) than in the VH-pol image (Figure 3b,d).

Figure 3. Dual-polarized RADARSAT-2 ScanSAR images in the Bay of Fundy (22:20 UTC, 14 May 2017): (**a**) VV-polarization, (**b**) VH-polarization, (**c**) VV-polarized sub-scene of the white box, and (**d**) VH-polarized sub-scene of the white box. RADARSAT-2 Data and Products MacDonald, Dettwiler, and Associates Ltd., All Rights Reserved.

*2.2. Surface Currents Detection Approach*

As shown in our previous study [9], the Bragg resonance plays a main role in the VV-polarized NRCS, but is negligible for the VH-polarization NRCS. Moreover, the non-Bragg scattering dominates

the VH-polarized NRCS, but is negligible for the VV-polarized NRCS. Because the sea surface Bragg waves on the scale of the microwave radar may interact with the surface currents, the radar signal due to Bragg resonance may therefore be modulated by the surface currents. Moreover, the strong currents in the Bay of Fundy are obviously captured by VV-polarization backscatter, but there are almost no features in the VH-polarized backscatter. A summary is presented in Table 1 for the roles of the above two main backscatter mechanisms with respect to the two different polarizations.

Table 1. The roles of the two mechanisms with respect to the two polarizations (VV & VH).

Mechanisms	VV-Pol	VH-pol
Bragg Resonance (Current modulation)	Main	Negligible
Non-Bragg (few current effects)	Negligible	Main

We propose an approach to detect surface current features from dual-polarized (VV and VH) SAR images based on assumptions that: (1) the VH-polarized NRCS is only induced by ocean wind; and (2) that the VV-polarized NRCS includes information related to both ocean winds and surface currents. Therefore, the approach is as follows: (1) retrieve wind vectors from the VH-polarized SAR image; (2) simulate the VV-polarized NRCS induced by wind by using the Bragg resonance mechanism (Equations (2) and (3)) and the non-Bragg scattering mechanism (Equation (4)); and (3) extract the ocean surface current features by removing the non-Bragg scattering contributions from the VV-polarized SAR image and by comparing the results to the simulated Bragg resonance NRCS. The approach is displayed in the flow chart in Figure 4.
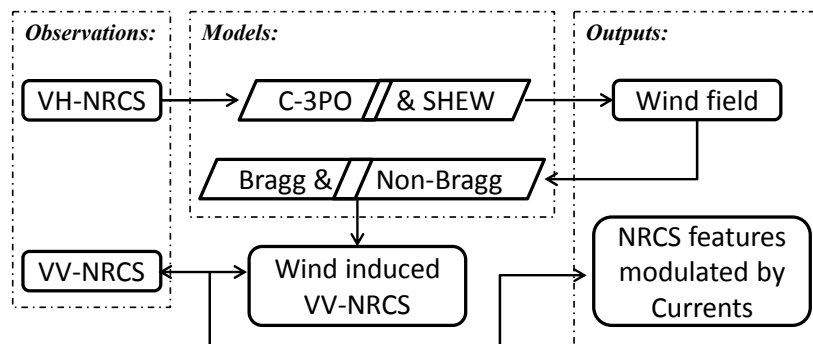

Figure 4. Flow chart for wind field retrieval and the backscatter features of surface currents.

After removing the non-Bragg scatter from the SAR VV-polarized NRCSs, we can estimate the surface currents by comparing the resultant NRCSs to the NRCSs resulting from the two-scale Bragg resonance. The flowchart in Figure 4 displays our approach including: (1) retrieval of wind fields from the VH-polarized images (Figure 2b), (2) simulation of two-scale Bragg resonance NRCSs, (3) extraction of the non-Bragg scattering, and (4) detection of ocean surface currents from VV-polarized NRCS data (Figure 2a). The backscatter features ($T_{current}$) of ocean currents are:

$$T_{current} = \frac{\sigma_{0VV} - \sigma_{0nb}}{\sigma_{oVV\_CB}} - 1 \tag{1}$$

where σ_{0VV} is the VV-polarized NRCS, as imaged by SAR (Figure 2a), σ_{oVV_CB} is the NRCS simulated by two-scale Bragg scattering (Equations (2) and (3)) by inputting the wind vectors that are retrieved from the VH-polarized NRCS, and σ_{0nb} is the Non-Bragg scattering (Equation (4)), which is independent of polarizations.

To calculate the Bragg scattering, we retrieve the wind speeds from the VH-polarized SAR image (Figure 2b) using the C-3PO (C-band Cross-polarization Coupled-Parameters Ocean) model [9], and we simulate the wind directions using the SHEW (Symmetric Hurricane Estimates for Wind) model [10] which is based on the typhoon structure. The wind vectors and retrieved wind speeds from the VH-polarized SAR image are shown in Figure 5a, as well as the reconstructed hurricane core structure in Figure 5b.
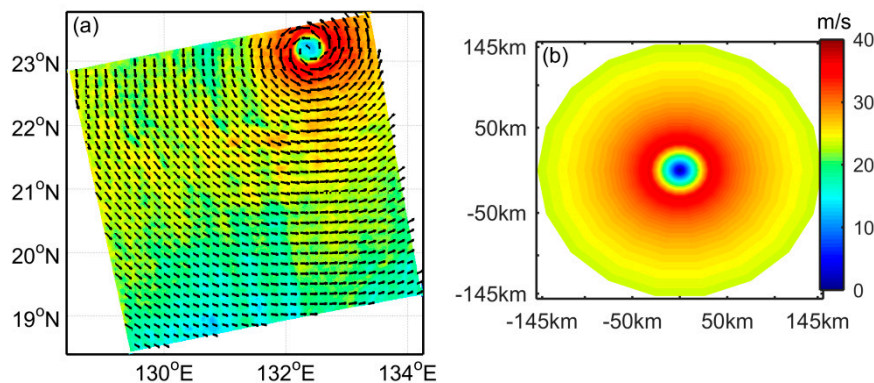
Figure 5. Wind vectors from a VH-polarized SAR image showing: (**a**) Wind speeds in color as retrieved by the C-3PO (C-band Cross-polarization Coupled-Parameters Ocean) model, and directions as estimated by the SHEW (Symmetric Hurricane Estimates for Wind) model; (**b**) Reconstructed wind speeds by the SHEW model.

2.2.1. Bragg Resonance Model

On the real ocean surface, the Bragg short waves run along the longer surface waves which change the local incidence angles and the local polarization relationship. Accounting for all of the possible surface tilting by using a probability density function (PDF) for the ocean surface slopes, we found that the two-scale Bragg scattering of the sea surface [16] is:

$$\sigma_{0VV\_CB}(\theta) = \int_{-\infty}^{+\infty} d(\tan\varphi) \int_{-\infty}^{+\infty} d(\tan\delta)\sigma_{0VV}(\theta_i)p(\tan\varphi, \tan\delta) \qquad (2)$$

where $p(\tan\varphi, \tan\delta)$ is the PDF of sea surface slopes which is described by a Gram-Charlier distribution [17] in this study, and $\sigma_{0VV}(\theta_i)$ is the backscattering cross section of a slightly rough patch for VV polarization as given by:

$$\sigma_{0VV}(\theta_i) = 16\pi k^4 \cos^4\theta_i \left| g_{vv}(\theta_i)\left(\frac{\alpha\cos\delta}{\alpha_i}\right)^2 + g_{hh}(\theta_i)\left(\frac{\sin\delta}{\alpha_i}\right)^2 \right|^2 W\left(K_{B_x}, K_{B_y}\right) \qquad (3)$$

where $W\left(K_{B_x}, K_{B_y}\right)$ is the wave spectrum induced by wind which may be modulated by the surface currents, g_{pq} are the Bragg scattering geometric coefficients for different polarizations [18], θ_i is the local incidence angle, $\alpha_i = \sin\theta_i$, $\alpha = \sin(\theta + \varphi)$, $\gamma = \cos(\theta + \varphi)$, and φ and δ are the angles of the tilting surface in the radar incidence plane and is perpendicular to the plane, respectively. The two wavenumber components of the Bragg resonance waves are $K_{Bx} = 2k\alpha$ and $K_{By} = 2k\gamma\sin\delta$. Here, the wind-wave spectrum follows that of Kudryavtsev et al. [19], which was adapted to calculate the wave spectrum in Equation (3) with the input of vector winds. Details of the parameters are given by [9] and [16]. With the retrieved wind vectors (Figure 5a) and model described in Equations (2) and (3), the VV-polarized NRCSs of the two-scale Bragg scattering signal are simulated, as shown in Figure 6a.
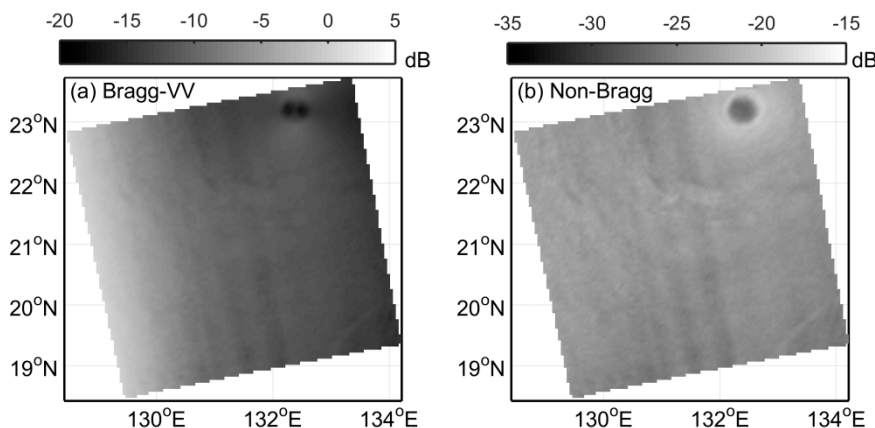
Figure 6. (**a**) Simulated VV-polarized NRCS by the two-scale Bragg model. (**b**) Simulated Non-Bragg scattering NRCS.

2.2.2. Non-Bragg Ratio

To describe the non-Bragg scattering mechanism, a phenomenological model was originally proposed by Phillips [20]. Thereafter, Kudryavtsev et al. [19] reviewed and simplified this non-Bragg model by using experimental results of Ericson et al. [21] and a conceptual approach of Wetzel [22]. Based on a high-quality database of five RADARSAT-2 dual-polarized (VV & VH) ScanSAR images collocated with aircraft observations obtained within a time window of ±30 min, we proposed a non-Bragg ratio [23]. Moreover, the Non-Bragg scattering is simulated here by:

$$\sigma_{0nb} = \frac{B_r}{1 + B_r} \cdot \sigma_{0VH} \tag{4}$$

where σ_{0VH} is VH-polarized NRCS imaged by SAR (Figure 2b), and B_r is the non-Bragg ratio with a constant value of 7.3. We note that the VV-polarized NRCS due to non-Bragg scattering is calculated using Equation (4) by also imputing the VH-polarized SAR image (σ_{0VH}). The reason for this is that the non-Bragg scattering (σ_{0nb}) is suggested to be independent of polarizations [9,19]. This implies that the non-Bragg scattering has the same values for VV or VH polarizations. Therefore, the VV-polarized (or VH-polarized) NRCSs values of the non-Bragg scattering (σ_{0nb}) are shown in Figure 6b.

3. Results

The surface currents' backscatter features that were detected from the dual-polarized SAR images at 09:20 UTC on 21 October are shown in Figure 7. The isoclines are from OSCAR five-day composite currents for 22 October. The OSCAR zonal and meridional currents, as well as the wind vectors from VH-polarization data are shown in Figure 8. The strongest OSCAR currents are in area A, which exceed 0.3 m/s. The surface current features that were extracted from the dual-polarized SAR images appear to agree with the strong currents in area-A. We also checked the OSCAR currents for October 17 and 27, where the strong currents continued to exist near area A. Figure 8 shows that the strongest currents are westward whereas the wind is towards the southeast. Thus, the currents tend to encounter the wind-waves and enhance the ocean surface roughness. Therefore, the SAR images reveal these strong current features.
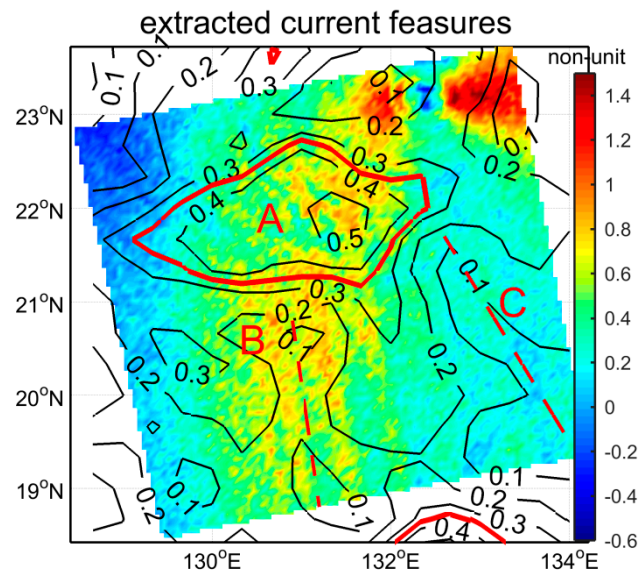
Figure 7. Ocean currents' manifestations (colors) from dual-polarized ScanSAR images. The isoclines are the OSCAR currents.
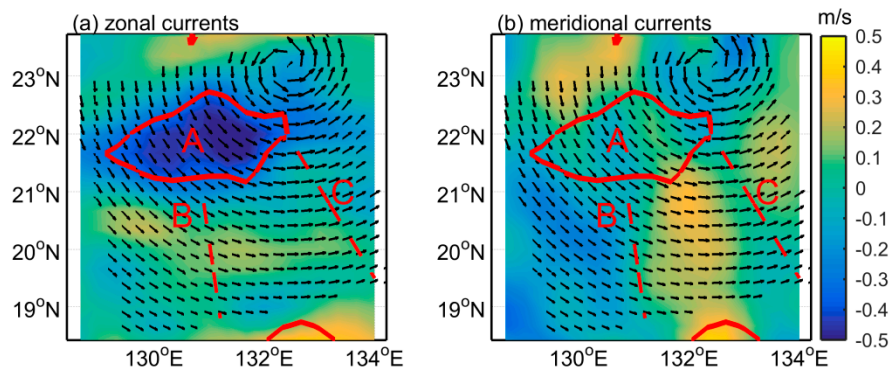
Figure 8. Decompositions of OSCAR currents in (**a**) zonal direction (positive is eastward and negative is westward); and (**b**) meridional direction (positive is northward and negative is southward). The wind vectors (black) as shown in Figure 5.

In Figure 7, the isoclines that are indicated by the red dashed line-B are similar to those of the red dashed line-C, whereas the backscatter features from SAR images near the two lines are totally different. These differences are due to the ocean current front along line-B where the meridional currents move in different directions, as shown in Figure 8b. Although the absolute values of the OSCAR currents around the two lines are similar, the directional distributions are different.

Thus, through these comparisons, we suggest that the backscatter features of the ocean currents extracted by our proposed approach correspond to the observed strong currents (>0.3 m/s) and the ocean front, even under TC conditions. Because it is difficult to distinguish the upper limits on the values in Figure 7 that were induced by strong currents and the ocean front, we therefore cannot apply this method to directly retrieve the ocean currents. However, this approach has the potential to provide validations of oceanic processes as simulated by numerical models, which is very important for the ocean studies [12], especially for high spatial resolutions. Moreover, as noted, OSCAR currents are 5-day composites, whereas SAR provides instantaneous snapshots with the typical revisit times being in the range of a few days. Thus, the high values for the current features around the typhoon eyes are not found in OSCAR currents, which may be induced by the high winds near the typhoon eyewall.

4. Discussion

The approach proposed in this study is based on: (1) our recent study investigating different mechanisms of the dual-polarized ScanSAR observations under TC conditions and (2) different observed features corresponding to the tidal currents in the Bay of Fundy for the different polarized channels (Figure 3). Although the results agree well with the 5-day composite currents from OSCAR retrieved from altimeters, there is still further study that is needed in order to retrieve precise estimates for surface currents from SAR images, especially under hurricane conditions. However, this approach provides insight into the SAR image through the strong wind signature that is generated by TC conditions, and also provides a methodology to extract surface current features by removing the strong wind signature.

Because of the strong characteristics that are related to extreme winds in TC conditions, the surface current features from the original VV-polarized SAR image (Figure 2a) are not as obvious as the low wind conditions in Figure 3a,c. However, when we remove the signal that is related to the winds from the VV-polarized SAR image, the extracted current features appear to agree with the 5-day composite OSCAR currents (Figure 7). The dominant current features (area A in Figure 7) represent the current modulations on the sea surface roughness generated by the wind, which demonstrates that the sea surface roughness can still be enhanced under extreme wind conditions. Regarding the oceanic feature around line-B, previous studies have suggested that it is a front under low or moderate winds [7,24].

Kudryavtsev et al. [5] indicated that the ocean surface current signatures are mostly dominated by non-Bragg backscatter through the analysis of the VV and HH polarizations from quad-polarized RADARSAT-2 SAR images. However, in this study, we remove the non-Bragg backscatter before extracting the current features. Our results are partly verified by the composite OSCAR currents and by our analysis, and the differences are due to spatial resolutions. The spatial resolution used here is about 5 km, compared to about 5 m in the azimuth direction for their studies.

Finally, heavy precipitation is always associated with typhoons and can attenuate the radar signal [23]. However, the surface current features around area A and line-B in Figure 7 are evident, which implies that these features are not due to rain, or that the rain rates around area A and line-B are not sufficiently high enough to obscure the modulations due to the currents in the C-band RADARSAT-2 dual-polarized (VV and VH) ScanSAR images.

5. Conclusions

To extract the current backscatter features imaged by SAR under extreme wind conditions, we propose an approach for C-band RADARSAT-2 dual-polarized (VV and VH) ScanSAR images. This approach is based on the fact that ocean winds and surface currents are both imaged by two channels at the same time (VV and VH). Because of the different roles of the two main backscatter mechanisms for the two different channels, we assume that the sea surface waves on the scales of the radar microwaves are modulated by the surface currents, and that these are only imaged by VV-polarization backscatter, and not by VH-polarization data. Thus, the process is simplified, and we retrieve the wind from VH-polarization backscatter and then extract the current features from the VV-polarization backscatter. Therefore, the dual-polarized ScanSAR mode makes it possible to detect the ocean surface features in the backscatter signal. Comparisons to the OSCAR currents from satellite altimeters suggest that the surface current features derived from SAR agree well with OSCAR currents under Typhoon Lan (2017) with extreme winds in regard to: (1) strong currents opposing the wind directions and (2) ocean fronts with opposing meridional directions.

We also note that although this approach extracts possible current features under extreme winds in Typhoon Lan (2017), it is still a simplified process that is based on the assumed approximation that the currents have no effect on the VH-polarized SAR image. With more observations and the development of backscattering theories, the relationship between the VH-polarized SAR image and ocean currents can be developed. However, the basic idea of this study remains meaningful that the two variabilities (winds and currents) can be detected using two different channel observations

simultaneously. The C-band Sentinel-1 SAR also has the dual-polarization (VV and VH) mode [25]. So, the approach or basic idea proposed here should possibly be applied to Sentinel-1 for ocean current feature detections.

Conflicts of Interest: The authors declare no conflict of interest.

Appendix A

The abbreviations used in this study are as following:

ADCP	acoustic Doppler current profiler
C-3PO	C-band Cross-polarization Coupled-Parameters Ocean
CSA	Canadian Space Agency
HF radar	High-frequency radar
NRCS	Normalized Radar Cross Section
OSCAR	Ocean Surface Current Analysis
PDF	probability density function
PO.DAAC	Physical Oceanography Distributed Active Archive Center
SAR	Synthetic Aperture Radar
ScanSAR	Synthetic Aperture Radar in Scan mode
SHEW	Symmetric Hurricane Estimates for Wind
TC	Tropical Cyclones
UTC	Coordinated Universal Time
VH	Transmits on Vertical (V) polarization but receives on Horizontal (H) polarization
VV	Transmits on Vertical (V) polarization receives on Vertical (V) polarization

References

1. Kang, K.M.; Kim, D.J.; Kim, S.H.; Moon, W.M. Doppler velocity characteristics during tropical cyclones observed using ScanSAR raw data. *IEEE Trans. Geosci. Remote Sens.* **2016**, *54*, 2343–2355. [CrossRef]
2. Li, X.; Zhang, J.A.; Yang, X.; Pichel, W.G.; DeMaria, M.; Long, D.; Li, Z. Tropical cyclone morphology from spaceborne synthetic aperture radar. *Bull. Am. Meteorol. Soc.* **2013**, *94*, 215–230. [CrossRef]
3. Chelton, D.B.; Schlax, M.G. Global observations of oceanic Rossby waves. *Science* **1996**, *272*, 234–238. [CrossRef]
4. Samelson, R.M.; Schlax, M.G.; Chelton, D.B. Randomness, symmetry and scaling of mesoscale eddy life cycles. *J. Phys. Oceanogr.* **2014**, *44*, 1012–1029. [CrossRef]
5. Kudryavtsev, V.; Kozlov, I.; Chapron, B.; Johannessen, J.A. Quad-polarization SAR features of ocean currents. *J. Geophys. Res.* **2014**, *119*, 6046–6065. [CrossRef]
6. Kudryavtsev, V.; Akimov, D.; Johannessen, J.; Chapron, B. On radar imaging of current features: 1. Model and comparison with observations. *J. Geophys. Res.* **2005**, *110*. [CrossRef]
7. Jones, C.T.; Sikora, T.D.; Vachon, P.W.; Buckley, J.R. Ocean feature analysis using automated detection and classification of sea-surface temperature front signatures in RADARSAT-2 images. *Bull. Am. Meteorol. Soc.* **2014**, *95*, 677–679. [CrossRef]
8. Liu, G.; Perrie, W.; Kudryavtsev, V.; He, Y.; Shen, H.; Zhang, B.; Hu, H. Radar imaging of intense nonlinear Ekman divergence. *Geophs. Res. Lett.* **2016**, *43*, 9810–9818. [CrossRef]

9.	Zhang, G.; Li, X.; Perrie, W.; Hwang, P.A.; Zhang, B.; Yang, X. A Hurricane Wind Speed Retrieval Model for C-Band RADARSAT-2 Cross-Polarization ScanSAR Images. *IEEE Trans. Geosci. Remote Sens.* **2017**, *55*, 4766–4774. [CrossRef]

10.	Zhang, G.; Perrie, W.; Li, X.; Zhang, J.A. A hurricane morphology and sea surface wind vector estimation model based on C-band cross-polarization SAR imagery. *IEEE Trans. Geosci. Remote Sens.* **2017**, *55*, 1743–1751. [CrossRef]

11.	Zhang, G.; Perrie, W. Effects of asymmetric secondary eyewall on tropical cyclone evolution in Hurricane Ike (2008). *Geophys. Res. Lett.* **2018**, *45*, 1676–1683. [CrossRef]

12.	Katavouta, A.; Thompson, K.R.; Lu, Y.; Loder, J.W. Interaction between the tidal and seasonal variability of the Gulf of Maine and Scotian Shelf region. *J. Phys. Oceanogr.* **2016**, *46*, 3279–3298. [CrossRef]

13.	Bonjean, F.; Lagerloef, G.S.E. Diagnostic model and analysis of the surface currents in the tropical Pacific ocean. *J. Phys. Oceanogr.* **2002**, *32*, 2938–2954. [CrossRef]

14.	RADARSAT-2 Product Description, 2014 MacDonald, Dettwiler Assoc., Richmond, BC, Canada, Tech. Rep. RN-SP-52-1238. Available online: https://mdacorporation.com/geospatial/international/satellites/RADARSAT-2 (accessed on 31 May 2018).

15.	Dalrymple, R.W.; Knight, R.J.; Lambiase, J.J. Bedforms and their hydraulic stability relationships in a tidal environment, Bay of Fundy, Canada. *Nature* **1978**, *275*, 100. [CrossRef]

16.	Hwang, P.A.; Zhang, B.; Toporkov, J.V.; Perrie, W. Comparison of composite Bragg theory and quad-polarization radar backscatter from RADARSAT-2: With applications to wave breaking and high wind retrieval. *J. Geophys. Res.* **2010**, *115*. [CrossRef]

17.	Cox, C.; Munk, W. Measurement of the roughness of the sea surface from photographs of the sun's glitter. *J. Opt. Soc. Am.* **1954**, *44*, 838–850. [CrossRef]

18.	Plant, W.J. Bragg scattering of electromagnetic waves from the air/sea interface. In *Surface Waves and Fluxes*; Geernaert, G.L., Plant, W.J., Eds.; Springer: Dordrecht, The Netherlands, 1990; pp. 41–108, ISBN 978-94-010-7429-2.

19.	Kudryavtsev, V.; Hauser, D.; Caudal, G.; Chapron, B. A semiempirical model of the normalized radar cross-section of the sea surface 1. Background model. *J. Geophys. Res.* **2003**, *108*. [CrossRef]

20.	Phillips, O.M. Radar returns from the sea surface-Bragg scattering and breaking waves. *J. Phys. Oceanogr.* **1988**, *18*, 1065–1074. [CrossRef]

21.	Ericson, E.A.; Lyzenga, D.R.; Walker, D.T. Radar backscatter from stationary breaking waves. *J. Geophys. Res.* **1999**, *104*, 29679–29695. [CrossRef]

22.	Wetzel, L. On microwave scattering by breaking waves. In *Wave Dynamics and Radio Probing of the Ocean Surface*; Phillips, O.M., Hasselmann, K., Eds.; Springer: Boston, MA, USA, 1986; pp. 273–284, ISBN 978-1-4684-8982-8.

23.	Zhang, G.; Li, X.; Perrie, W.; Zhang, B.; Wang, L. Rain effects on the hurricane observations over the ocean by C-band synthetic aperture radar. *J. Geophys. Res.* **2016**, *121*, 14–26. [CrossRef]

24.	Li, C.; Li, X.; Zhang, G.; Boswell, K.M.; Kimball, M.E.; Shen, D.; Lin, J. Estuarine Plume: A Case Study by Satellite SAR Observations and In Situ Measurements. *IEEE Trans. Geosci. Remote Sens.* **2017**, *55*, 2276–2287. [CrossRef]

25.	Velotto, D.; Bentes, C.; Tings, B.; Lehner, S. First comparison of Sentinel-1 and TerraSAR-X data in the framework of maritime targets detection: South Italy case. *IEEE J. Ocean. Eng.* **2016**, *41*, 993–1006. [CrossRef]